Mechanics and Mechanical Engineering
Vol. 22, No. 1 (2018) 7–23

https://doi.org/10.2478/mme-2018-0001

Experimental Validation of a Novel Thin-Walled Beam Prototype

Hugo Miguel Silva
José Filipe Meireles
Department of Mechanical Engineering, University of Minho
Campus of Azurém
4800-058 Guimarães, Portugal
hugolopessilva@gmail.com
meireles@dem.uminho.pt

Jerzy Wojewoda
Division of Dynamics, Lodz University of Technology
Stefanowskiego 1/15, 90-924 Łódź, Poland
jerzy.wojewoda@p.lodz.pl

Received (17 July 2017)
Revised (20 March 2018)
Accepted (20 April 2018)

In this paper, an experimental validation of a novel beam prototype is performed. Tensile tests, both until rupture and on the elastic domain were done in order to determine the material properties. They were used then in Finite Element Analysis model built in *ANSYS Mechanical APDL*. Three experimental tests were done to the prototype, and, in order to minimize errors, the average value of the three tests determined, and compared with results obtained from the numerical model. It was shown that it was possible to manufacture the beam by the presented manufacturing methodology. An acceptable correlation between the numerical an experimental results was found.

Keywords: Sandwich beams, Mechanical behaviour, FEM, Finite Element Method, Solid Mechanics, steel beam, sheet steel beam

1. Introduction

The acceleration of industrial machines mobile parts has been increasing over the last few years, due to the need of higher production in a short period of time. The machines were dimensioned for a lower value of acceleration, which means there is not enough rigidity for the correct operation at larger accelerations. Nowadays, it can be near 12 times higher than the acceleration of gravity. There is the need of improving rigidity to make possible the correct machine operation without undesired vibrations that can ultimately lead to failure [1, 2]. Having these considerations in mind, effective geometries have already been studied and similar geometries to

the prototype of this work were tested for feasibility [3]. Parameters that allowed effectiveness comparison between different kinds of all-metal sandwich beams were already established [4, 5]. In this work, considered models were earlier optimized using a Sequential Quadratic Programming (SQP) code, built in MATLAB. Very few works were found regarding the mechanical behaviour of stiffened structures. Liu developed a reinforcement methodology for thin-walled steel beams that can increase bending and torsion strength and without any increase in the weight of the objects [6]. Liu and Gannon focused on reinforcing a W-shaped steel beam with welded plates under load [7]. The FEM was used for its modeling with the finality of investigating the effect of some parameters related to the process, namely reinforcing patterns, preload magnitudes at the time of welding, and initial imperfections of the unreinforced beam.

Szewczak et al. studied the influence of four types of stiffeners on three types of beams support: pin ended, fix ended and cantilevered [8]. The beams were subjected to either concentrated or distributed torques. Both the quantity and the location of the stiffeners were changed. The authors developed design recommendations on the type of stiffener, the size, and the placement. Heins and Potocko predicted the torsional response of box stiffened I-sections by two analytical procedures [9]. These methods utilize basic torsion theory and compatibility relationships. However, none of these studies shown a manufactured prototype, neither an experimental setup that allows testing under unsymmetrical transverse loadings.

Magnucka-Blandzi and K. Magnucki [10] studied a simply supported sandwich beam which has a metal foam core. The mechanical properties of the core vary across its depth. The authors formulated a nonlinear hypothesis of deformation of a plane cross section, which is assumed and described therein, and determined the stress state and the critical force for the studied beam. Grygorowicz et al. [11] studied the elastic buckling behavior of a three-layered beam with metal foam core by analytical and numerical methods. The finite elements analysis performed by the authors used a linear elastic buckling model. The authors analyzed beams with either constant or variable Young's modulus of the core of the beam. The values of the critical load obtained by the analytical and numerical(FEM) methods are compared and discussed by the authors.

Magnucki et al. [12] studied mono- and anti-symmetrical open I-sections of cold-formed thin-walled beams having double flanges. The beams were loaded with a uniformly distributed vertical load and simply supported at both ends boundary condition was applied. The geometric properties of each of the I-sections are described separately by dimensionless parameters. The authors defined parameters related to strength, global and local buckling. A dimensionless objective function is formulated and implemented as the optimization criterion. The paper presents graphical results of a numerical study of a family of thin-walled beams. Magnucki [13] studied cold-formed thin-walled beams with open cross section. The beam cross section is optimized considering a fixed cross section area and having strength and stability constraints. Optimal geometrical parameters of the cross section in terms of maximal and safe bending moment were determined. In the study, the considered strength condition is a classical one, that was applied to the beam theory for the assumed allowable stress. Results present the numerical analysis, including examples of optimal cross sections of the thin-walled beams.

2. Experimental Procedure

2.1. *Tensile Test: Experimental aspects*

The tensile test was performed on an Instron 8874, having a load capacity of 25 kN, Fig. 1. The data acquisition system used was SPIDER8. The system read the electrical signal coming from the extensometer. The system was controlled via the PC software *CATMAN*, which allowed collecting and saving relevant data from the test, such as normal and transversal extensions. The specimen were fixed along their transversal area at the ends. The fixtures have rough zones that hold the specimen in place. During the tensile test, an electromechanical extensometer was used while load remained in the elastic domain. In the extensometry tests, the measurements are done individually, with 2 strain-gauges, in 90° to each other, with each strain-gauge having a one-quarter of WheatStone bridge. Both strain-gauges were reusable, as long as the plastic zone has not been reached during a test. If the plastic zone was reached, the extensometer would present a permanent residual extension, which could affect the accuracy of the results on later tests.

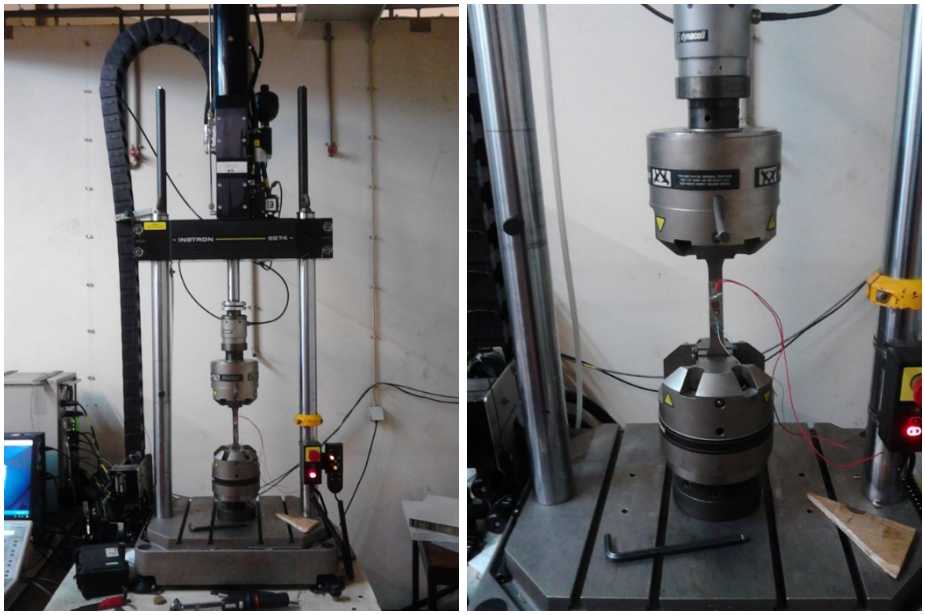

Figure 1 Instron Test Machine (left) and specimen during the extensometry test (right)

Table 1 Chemical composition of electrogalvanized DC01, tested by tensile test, according to the supplier

%Fe	%C	%Mn	%P	%S
99.574	0.075	0.310	0.021	0.020

The specimen were made by cutting a sheet with 1 mm thickness of the steel of the grade DC01, previously galvanized, for which the chemical composition is shown in Tab. 1. Six specimens were cut, and three of them were tested. The specimens were named according to the direction of cut: the A and B specimens were cut on a direction of 90° in relation to each other. Two types of tests were done: a test until rupture and another only in the elastic domain, the latter known as extensometry. The rupture test was performed with two specimens, named A1 and B1, Fig. 2. In this test, an electromechanical extensometer brand TML, model QFCA-3 mm, having an internal resistance of 120 Ohm, was coupled to the machine at low loads, for accurate determination of the Young's modulus. The test was performed with two deformation speeds: $v_1 = 0.01$ mm/s until a deformation of 1 mm and $v_2 = 0.2$ mm/s from then until the end of the test. The extensometry test was made only on the A2 specimen. In this test, two extensometers were bonded to the specimen at 90° in order to measure the extensions in the longitudinal and transversal directions. This is needed to calculate the Poisson coefficient, which is important for the definition of material properties in the FEM model when comparing experimental and numerical results, Fig. 3.

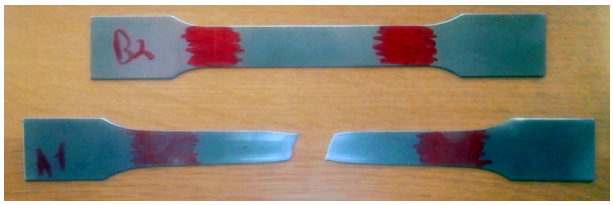

Figure 2 Non-tested specimen (top) and specimen A1 tested to the rupture after test (bottom)

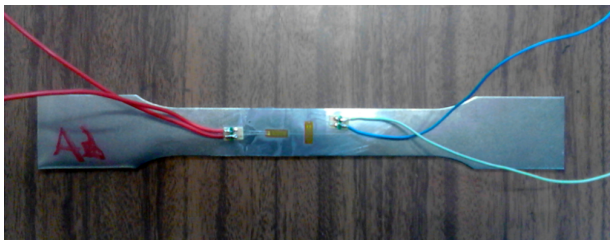

Figure 3 A2 specimen tested in extensometry test, along with two perpendicular electric extensometers

2.2. *Prototype test*

2.2.1. *Numerical model*

The material properties are as shown in Table 2. The material was considered to be orthotropic, with the values of Young's modulus obtained in the tensile test. E_z is considered to be the longitudinal rolling directions, and, as such, has the higher Young's modulus value. E_x and E_y are considered to be the transversal directions. It was not possible to observe, by looking at the sheet specimens, which

Table 2 Mechanical properties of the steel used in the simulation and on the experimental test

Property	*Value*
Young's modulus	$E_z = 199.3 \cdot 10^9$ [Pa] $E_x = E_y = 176.2 \cdot 10^9$ [Pa]
Poisson coefficient	0.323
Density	7890 [kg/m^3]

was the longitudinal rolling direction. However, the beam is constructed with sheets oriented in many directions, which makes the assumption of any direction to be the longitudinal to be a simplification. Assumed FEM element type was SHELL63 for the entire model. The mesh was a quadrilateral free mesh, with elements with 0.0025 m of mean element size. The mesh is shown in Fig. 4. The results were queried at one keypoint named P1 and shown in Fig. 5.

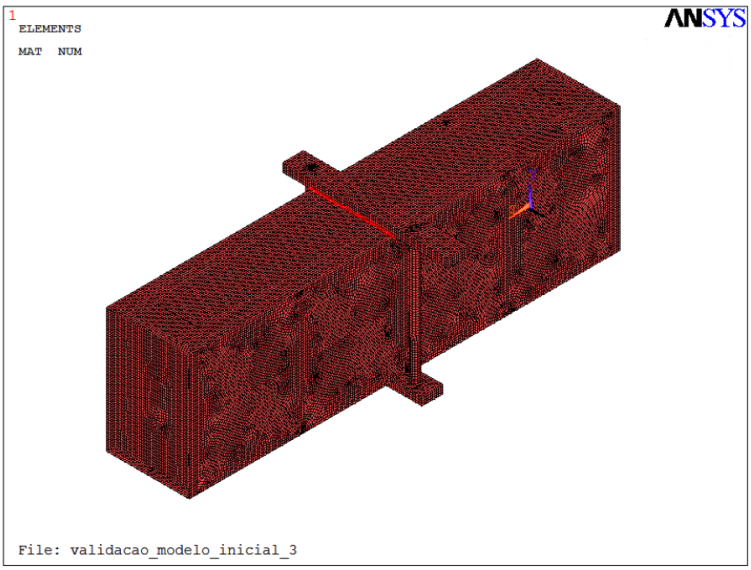

Figure 4 Mesh of the FEM model of the prototype

Contact was simulated between the bottom surface of the loaded plate, as well as the top surface of the plate located on the opposite side (bottom) and the beam. A surface to surface contact pair was created in *ANSYS MECHANICAL APDL*. TARGE170 elements were assigned to the volumes of the bar located at the top, and CONTA174 elements were assigned to the contacting areas on the prototype. The beam was only constrained as simply supported in the numerical model due to the fact that during the test the experimental beam prototype is simply supported at both ends, see Fig. 6. The rods/plate systems at both sides of the beam, shown there, were clamped to the bottom of the support. This ensures that the

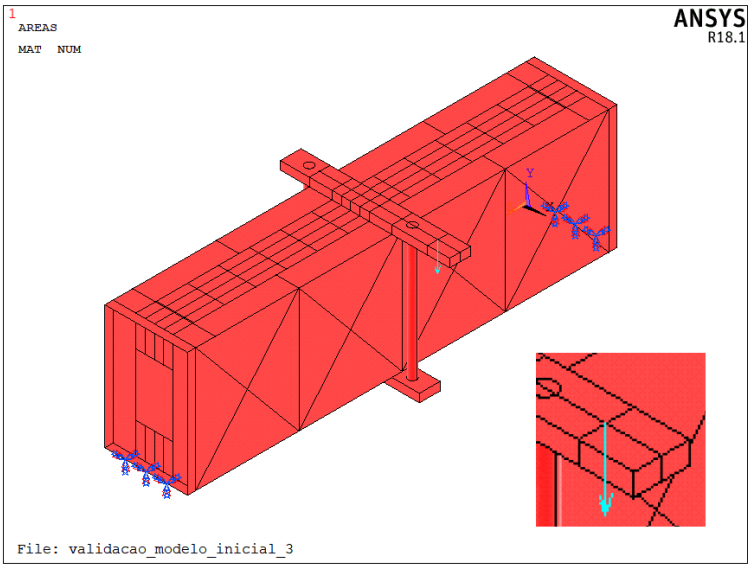

Figure 5 Geometry of the numerical model with the points where validation results were queried, as well as the applied load and DOF constrained applied to the areas of the ends

beam is constrained enough for the experimental test to be reliable and safe. The clamped rod/plate systems, by simplification are not considered in the simulation, due to the difficulties in creating complex geometries in *ANSYS APDL*, and the modelling in the *INVENTOR* software could result in importing problems, especially when the geometry was read into *ANSYS*. The model was built as a solid model in *AUTODESK INVENTOR*. Due to the high effect of torsion, originated by unsymmetrical loading, particularly present at the ends of the beam, to constrain the beam at the end will lead to unrealistic results, because the contact between the surfaces is far from perfect.

2.2.2. *Experimental setup*

The experimental setup is shown in Fig. 6. Due to manufacturing constraints of the beam, it is expected that the deflections measured by the dial indicator in the experimental work would be higher than those obtained by FEM software. This happens due to the imperfect connection between welded surfaces of the prototype, while the software consider perfect contact between all the contacting zones.

2.2.3. *Beam prototype physical model*

In this section, pictures of the laser cut sheet metal beam components are shown after laser cutting and before welding in Figs. 7–12.

The manufactured beam is shown in Figs. 13 and 14. The steel sheets shown in the previous section were assembled and Tungsten Inert Gas (TIG) welded.

The computer aided design (CAD) model was built in *Autodesk Inventor Professional 2015*. The model comprises two types of geometries: internal reinforcements

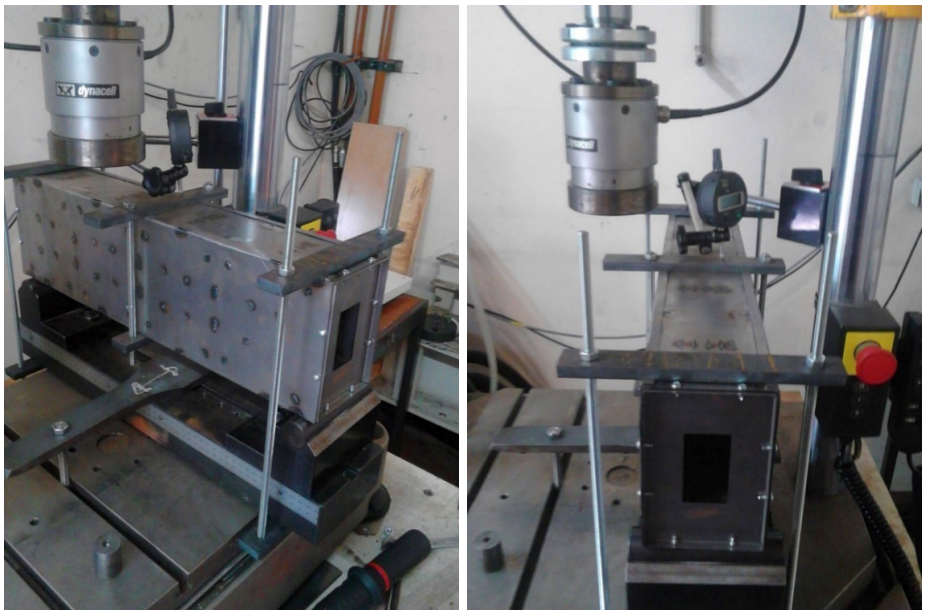

Figure 6 Beam prototype and experimental setup: isometric view (left) and section view (right)

Figure 7 Laser cut sheet of the component 101

Figure 8 Laser cut sheet of the component 102

Figure 9 Laser cut sheet of the component 103

1, and connecting plates 2. All the 1 parts had reentrances that connect to 2, which have holes with tolerances of 0.2 mm in relation to the dimensions of the reentrances in the longitudinal direction of the hole and 0.1 mm in the other one. Both had rectangular geometry. This practical consideration allowed welding places which would be otherwise inaccessible, such as the welding of the outer plates (Figs. 13 and 14). An example of this consideration is shown in Fig. 15.

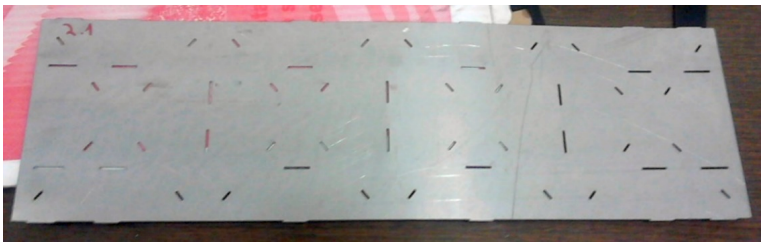

Figure 10 Laser cut sheet of the component 104

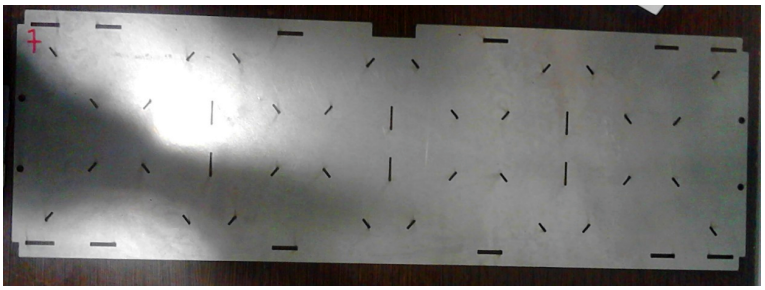

Figure 11 Laser cut sheet of the component 105

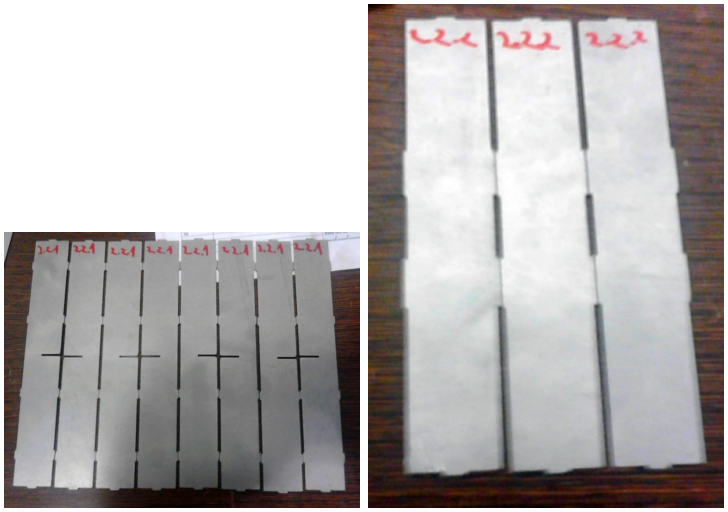

Figure 12 Laser cut sheet of the component 110 (left) and of the component 110B (right)

Manufacturing process of the beam comprised of three main steps: sheet steel cutting, assembling, and welding. Sheet steel cutting was realized by supplying the `.dxf` files originating from CAD models to the machine. Native Autodesk Inventor Solid part models (`.ipt` files) were converted to `.dxf` or `.dwg` files, which the laser cutting software can read. Assembling of the models was done as instructed to the workers at the workshop. By the time of manufacturing, an assembly was already

Figure 13 Section view of the welded beam (left) and its isometric view (right)

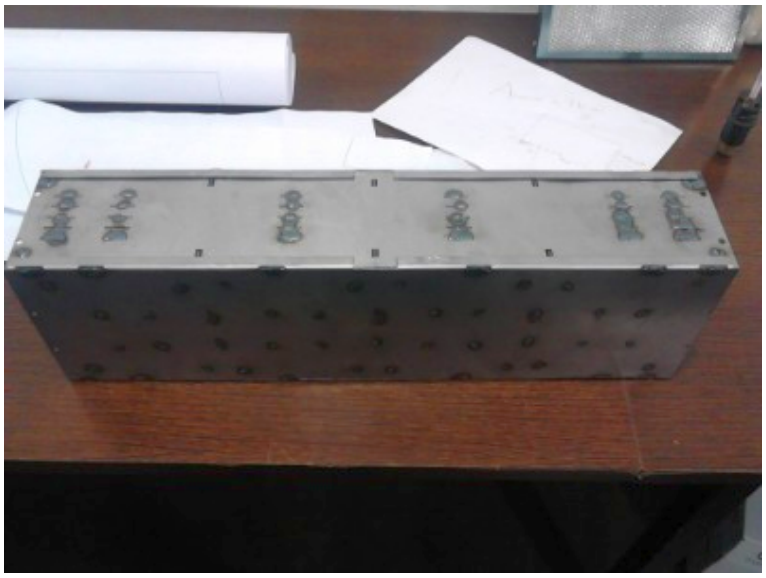

Figure 14 Top/side view of the welded beam

done in the CAD program to be able to test the tolerances, learn about the order in which parts are assembled, and ensure that each of the individual parts had correct dimensions prior to the manufacturing. Welding was done for each connecting pair right after the guidance about the correct placement of the part in the assembly and the specific order of the parts. Each of the individual parts was assembled into a set, as described above. The assembly is shown in Figs. 13 and 14. It is composed of

Figure 15 Connection of parts of type 1, (shown in blue) and 2 (shown in red). The loosening allows enough room for joining the parts by Tungsten Inert Gas (TIG) welding, but at the same time, it is possible to have good cohesion

6 different parts, some of which are used in multiple quantities, as shown in Table 3.

Table 3 Quantity of each of the individual parts on the assembly

Part designation	*Quantity*
101	2
102	6
103	2
104	2
105	2
110	2

The apparatus used for the experimental test is shown earlier in the Fig. 6. There were 3 groups of pairs of plates shown there, each of which were connected by two nuts on each of the extremities and two "rods". The two groups are located at the extremities, and one in the center. Two screws were attached to the machine, with a sheet bar constraining movement of the support during the test. The group located in the centre was fixed to the lower side of the support. The aim of the top sheet was to allow the application of an unsymmetrical bending load, which is equivalent to a bending and torsion coupled load. A dial indicator was used to measure the displacement at the point P1. The dial indicator had a a sensitivity of 1 μm. The load was applied on a distance of 0.04 m to the edge of the beam in the direction of the beams width.

In order to reduce the effect of the reaction at the supports on the prototype, two parts were used at both sides of the ends, as presented in Fig. 6. Eight screws were used at each side, two on each face, to fix them. These parts were not included in the numerical model (Fig. 20) due to the fact that *ANSYS* considers perfect connections between every geometrical element: such as points, lines, areas and volumes. The difference between the conditions of the numerical model and experimental one, in terms of manufacturing, may have led to some discrepancy in the results. Despite this fact, all other conditions were reproduced all similarly as possible by the numerical and experimental method, in order to avoid further discrepancy on the results, see Tab. 7.

3. Calculations

3.1. *Tensile test*

During the tensile test, results were obtained as a `.raw` file that was later opened in Microsoft Excel. The relevant results contained time [s], extension [mm], strain [%], and load [N], but more results were obtained, such as toughness and true stress. The results were automatically sorted by time instant. The estimative of Young's modulus was obtained by selecting the elastic part of the stress-strain curve and performing a linear fit, such as in Fig. 19. The determination of the yield strength was done by adding a straight line to the stress-strain chart. The straight line is parallel to the initial straight zone of the stress-strain chart and crosses the y-axis (stress) at $x = 0.2\,\%$, as in Figs. 17 and 18 [14].

3.1.1. *Extensometry test*

It is possible to calculate the nominal stress by dividing the load by the transversal area of the specimen, as in [14]

$$\sigma = \frac{F}{A}\,, \tag{1}$$

where σ is the normal stress, F the applied load and A the transversal area of the specimen.

In order to determine Young's modulus, one must do the linear fit of the stress-strain chart for the elastic domain data. The equation used to perform the linear fit is:

$$y = sx + b_C\,, \tag{2}$$

where x and y were the coordinates, s is the slope of the line, and represented the Youngs modulus value, b_c is the y coordinate on origin. It is, however, highly recommended to choose an interval of data that is not too close to the beginning of the stress-strain chart, due to the measuring instability of the machine, and also not too far from the beginning, to avoid selecting data on the plastic domain, obtaining then an erroneous approximation of the Young's modulus. The Poisson coefficient was determined by [15]

$$\nu = -\frac{\epsilon_{trans}}{\epsilon_{long}}\,, \tag{3}$$

in which both the transversal and longitudinal strains are obtained via the electrical extensometers.

4. Results

4.1. *Tensile tests*

4.1.1. *Rupture test*

Data collected during this test create stress-strain curve for the specimens tested until rupture which is shown in Fig. 16. For determination of yield strength, a straight line having the same slope as the elastic part of the stress-strain curve was plotted with it. The y coordinate of the intersection between the two curves is the yield strength. The charts are shown in Fig. 17 (for the specimen A1) and Fig. 18 (for the specimen B1).

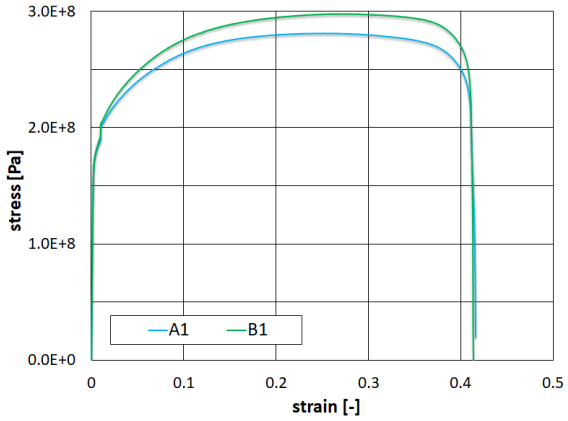

Figure 16 Stress-strain curve for the specimens A1 and B1, tested until rupture

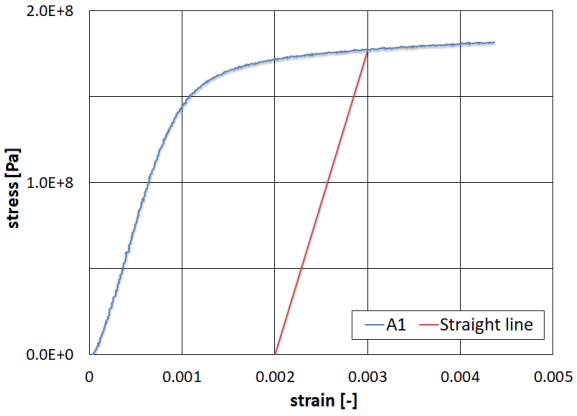

Figure 17 Determination of the yield strength for the specimen A1

For estimation of the Young's modulus, a linear fit was done in the elastic domain. The points were chosen in a range that is on the elastic domain, but without the errors that may occur in the beginning of the test, neither with the risk of being too close to yield. Figure 19 show the determination of Young's modulus for the specimens A1 and B1. The results presented in Figs. 17–19 have been summarized in the Table 4.

Table 4 Yield stresses and Young's modulus obtained in tensile test

Specimen	yield stress [Pa]	Young's modulus [Pa]
A1	$176.6 \cdot 10^6$	$176.2 \cdot 10^9$
B1	$178.4 \cdot 10^6$	$199.3 \cdot 10^9$

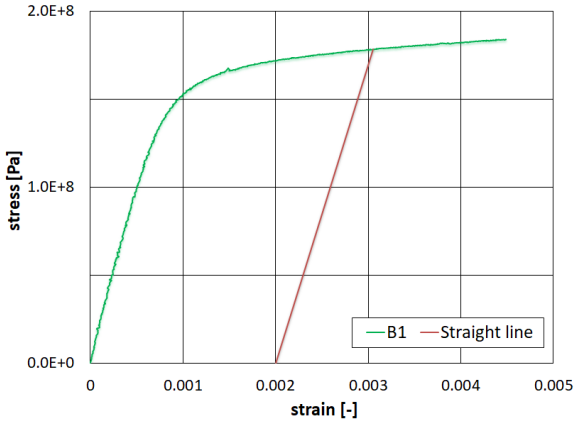

Figure 18 Determination of the yield strength for the specimen A2

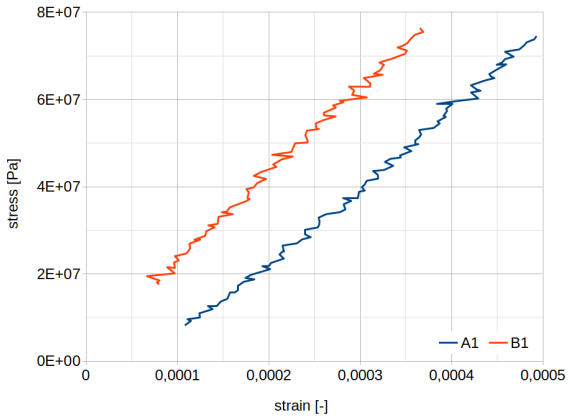

Figure 19 Determination of the Young's modulus for the specimen A1 and B1

The elongation of the tested specimens was determined by the change in length of the L_i during the test, and measured after the test L_f is shown in Table 5.

Table 5 Final engineering strain determined by the tensile test

	L_i [mm]	L_f [mm]	e_{strain}
A1	100.0	138.5	0.385
B1	100.0	137.0	0.370

4.1.2. *Extensometry test*

The extensometry test was done with displacement speed of 0.01 mm/s and its results has been summarized in Table 6.

Table 6 Final engineering strain determined by the tensile test, as well as proof stresses

time [s]	F [N]	σ_{long} [–]	σ_{trans} [–]	ν	stress [Pa]	E [Pa]
6.1	1007.8	257.28	−80.88	0.314	$5.08 \cdot 10^7$	$1.87 \cdot 10^{11}$
8.9	1499.4	405.60	−132.00	0.325	$7.55 \cdot 10^7$	$1.86 \cdot 10^{11}$
11.7	2002.7	546.72	−181.20	0.331	$1.01 \cdot 10^8$	$1.84 \cdot 10^{11}$

4.2. *Prototype test*

Figure 20 shows the global y deflection values obtained in *ANSYS Mechanical APDL* and presented as a colour scaling for the numerical model used for the validation.

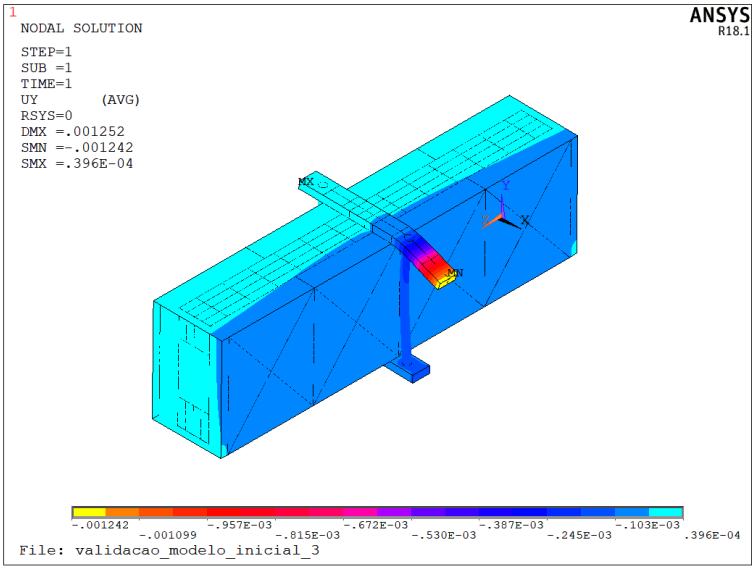

Figure 20 y deflection results obtained in ANSYS MECHANICAL APDL for loading of 2000 N

The numerical results were compared to those collected during the experiments. The deflections obtained in both methods are shown in Table 7. On the experimental method, results were read from the dial indicator. Three experimental tests named exp1, exp2 and exp3, were done in order to minimize measuring errors. The numerical results has been presented as δ_{num}.

Here, deflections are: δ_{num} in numerical method on *ANSYS MECHANICAL APDL*, δ_{expi}, $i = 1, 2, 3$ in experimental method on the i-th test and δ_{expAvg} mean, experimental value. Errors, expressed in percent, were relative differences between

Table 7 Comparison of experimental and numerical results

Load [N]	1500	2000
δ_{num}	$3.01 \cdot 10^{-6}$	$4.01 \cdot 10^{-6}$
δ_{exp1}	$5.00 \cdot 10^{-6}$	$6.00 \cdot 10^{-6}$
δ_{exp2}	$2.00 \cdot 10^{-6}$	$2.00 \cdot 10^{-6}$
δ_{exp3}	$1.00 \cdot 10^{-6}$	$4.00 \cdot 10^{-6}$
δ_{expAvg}	$2.67 \cdot 10^{-6}$	$4.00 \cdot 10^{-6}$
error [%]	12.9	0.2

the numerical and experimental methods given by:

$$\text{error} = \frac{\delta_{num} - \delta_{expAvg}}{\delta_{expAvg}} \cdot 100\% \,. \tag{4}$$

The results variation, in the case of experiment, are mainly caused by the precision of the dial indicator used. In fact, it has precision of $1 \cdot 10^{-6}$ m (1μm). This means that taking results a little before or after the experimental testing machine reaches the proof loads of 1500 N or 2000 N may originate a variation of the results. For this reason, three experimental tests were done, in order to improve the accuracy of the results by comparing the average values of the experimental tests with the numerical ones.

5. Discussion of results

5.1. *Tensile tests*

The stress-strain chart in Fig. 16 shows a typical stress-strain curve, with the specimen B1 having higher rupture stress and yield stress in comparison with A1. The elongation reached near 40% for both specimens. The yield stress presents relatively low value when compared to most of other kinds of steels. This confirms that the tested material is a low-alloy steel due to its relatively low resistance and high elongation, what also means that the material has high ductility. The specimen B1 has the characteristics of a longitudinal type when compared to A1, according to Fig. 16. The value of the Young's modulus also confirms that the specimen B1 was cut on the direction of the previous sheet deformation that occurred in the rolling processes. Such a process deforms the grains along the direction of the rolling, therefore originating different mechanical properties in comparison with the transversal direction [16]. This is due to the higher value of the Young's modulus obtained for the specimen B1 (199.3 GPA) in comparison with A1 (176.2 GPA). The value of the yield stress is higher for specimen B1 (182.2 MPa) in relation to A1 (180.5 MPa). This also confirms that specimen B1 is the longitudinal one. The Poisson coefficient obtained from the extensometry test was between 0.315 and 0.331.

5.2. *Prototype testing*

Regarding the experimental validation of the prototype, the results correlation between the experiment and numerics were declared acceptable, specially considering the average results of the three experimental tests. Factors such as tolerances of the manufactured part may have a role on the results discrepancy, but the most important factor is the fact that the manufactured part is welded at only part of the surfaces, while the numerical model has perfect contact between the surfaces. As the model is transversely loaded in the direction of the axis of the highest axial inertia moment, the difference is less meaningful than if the model was loaded in other directions.

6. Conclusions

The experiments performed on the samples of material used delivered the following conclusions:

- Specimens A1 and B1 differed on the rupture stress, Young's modulus, and slightly on yield stress, but there was not a significant difference on the maximum elongation. Specimen B1 is the longitudinal specimen, while the A1 is the transversal one.
- Values of the Young's modulus obtained in both tensile and extensometry tests delivered very reasonable results when compared to the typical reference value for such material, which is 200 GPa [16].
- Values of the Poisson coefficient obtained in the extensometry test confirms the reference value of 0.33 [16].

Testing of the prototype allowed for the following statements:

- It was possible to manufacture the thin-walled beam prototype presented in this paper. All the dimensions were reduced to half of those considered in previous works, such as in [3], included the thickness. However, in this work, the numerical model has the same dimensions as the prototype, in order for the comparison to be possible. This allows ease of transportation thanks to its lower weight and volume.
- The experimental setup allowed to constrain the prototype correctly during the test, without any noticeable excessive translation or rotational movement.
- The results showed an acceptable correlation between numerics and experiments. The absence of welding in most of the area of the connecting surfaces may be the most significant source of the errors that occurred in the correlation of the numerical and experimental results, as it is shown in Tab. 7.

The work, although performed using basic tests, allowed to validate the numerical approach obtained by Silva and Meireles with experimental results [3, 17].

References

[1] Silva, H.M., De Meireles, J.F.: Determination of material/geometry of the section most adequate for a static loaded beam subjected to a combination of bending and torsion, *Materials Science Forum*, 730–732, (2013), 507–512.

[2] Silva, H.M.: *Determination of material/geometry of the section most adequate for a static loaded beam subjected to a combination of bending and torsion*, MSc. Thesis, University of Minho, (2011).

[3] Silva, H. M., De Meireles, J. F.: Feasibility of Internally Reinforced Thin-Walled Beams for Industrial Applications, *Applied Mechanics and Materials*, 775, (2015), 119–124.

[4] Silva, H. M., De Meireles, J. F.: Effective Mechanical Behavior of Sandwich Beams under Uncoupled Bending and Torsion Loadings, *Applied Mechanics and Materials*, 590, (2014), 58–62.

[5] Silva, H. M., De Meireles, J. F.: Effective Stiffness Behavior of Sandwich Beams under Uncoupled Bending and Torsion Loadings, *Applied Mechanics and Materials*, 852, (2016), 469–475.

[6] Liu, Y., Design enhancement of thin-walled steel beams with improved stiffness and reduced weight, International. *Journal of Design Engineering*, 1(2) (2008), 149–165.

[7] Liu, Y., Gannon, L., Finite element study of steel beams reinforced while under load, *Engineering Structures*. 31, (2009), 2630–2642.

[8] Szewczak, R., Smith, E., and DeWolf, J., Beams with Torsional Stiffeners, *Journal of Structural Engineering*, 109:7, (1983), 1635–1647.

[9] Heins, C. P. Jr., and Potocko, R. A., Torsional Stiffening of I-Girder Webs, *Journal of the Structural Division*. ASCE, 105, ST8, (1979), 1689–1698.

[10] Magnucka-Blandzi,E., Magnucki, K. Effective design of a sandwich beam with a metal foam core, *Thin-Walled Structures*. 45 (2007) 432–438.

[11] Grygorowicz, M., Magnucki, K., Malinowski, M., Elastic buckling of a sandwich beam with variable mechanical properties of the core, *Thin-Walled Structures*. 87 (2015) 127–132.

[12] Magnucki,K., Rodak,M., Lewinski,J., Optimization of mono- and anti-symmetrical I-sections of cold-formed thin-walled beams, *Thin-Walled Structures*. 44 (2006) 832–836.

[13] Magnucki,K., Optimization of open cross section of the thin-walled beam with flat web and circular flange, *Thin-Walled Structures*. 40 (2002) 297310

[14] Stefanescu, D. M.: *Handbook of Force Transducers*, Springer Link, (2011).

[15] Beer, F. P. Jr., Johnston, E. R., DeWolf, J. T: *Mechanics of Materials*, 3rd Edition McGraw-Hill, (2001).

[16] Smith, W. F.: *Princpios de ciência e engenharia dos materiais*, 3rd Edition, McGraw Hill, (1996).

[17] Silva H.M., Meireles J.F, 2017a Structural Optimization of internally reinforced beams subjected to uncoupled bending and torsion loadings for industrial applications, *Mechanics and Mechanical Engineering*. 21(2), (2017) 329–351.